Hindawi
Journal of Nanomaterials
Volume 2022, Article ID 4743040, 8 pages
https://doi.org/10.1155/2022/4743040

Research Article

Highly Sensitive H_2 Sensors Based on Co_3O_4/PEI-CNTs at Room Temperature

Laixu Gao,[1] **Songquan Li**,[1] **Xiaoxue Xu**,[2] **Changwei Zou**,[1] **and Guo Zhang**[3]

[1]*School of Physics Science and Technology, Lingnan Normal University, Zhanjiang 524048, China*
[2]*School of Biomedical Engineering, Faculty of Engineering and Information Technology, University of Technology Sydney, NSW 2007, Australia*
[3]*School of Chemical Engineering and Material, Heilongjiang University, Harbin 150080, China*

Correspondence should be addressed to Laixu Gao; gaolaixu@lingnan.edu.cn

Received 21 October 2021; Revised 26 December 2021; Accepted 11 January 2022; Published 29 January 2022

Academic Editor: Zhi Li Xiao

The highly dispersed Co_3O_4 on the surface of CNTs modified with polyethylenimine (PEI) was synthesized using the hydrothermal method. In the CNT-Co_3O_4 composite materials, CNTs not only provide the substrate for the Co_3O_4 nanoparticles but also prevent their aggregation. Furthermore, the interaction between Co_3O_4 and CNTs modified with polyethylenimine (PEI) helps to improve the gas sensing performance. In particular, the CNT-Co_3O_4 composite synthesized at 190°C shows the outstanding sensitive characteristics to H_2 with a lower detection limit of 30 ppm at room temperature. The obtained CNT-Co_3O_4 sensor displays excellent selectivity and stability to H_2. The energy band model of the conductive mechanism has been built to explain the resistance change when the gas sensor is exposed to the H_2. Hence, the CNT-Co_3O_4 composite material presents highly promising applications in H_2 gas sensing.

1. Introduction

Hydrogen energy is the most ideal clean and renewable energy with high heating value, so it is widely used in spacecraft, fuel cell, and internal combustion engine fuel [1–4]. Hydrogen can be stored in the form of gas, liquid, or even solid metal hydrides; thus, the hydrogen can be very potentially convenient to be employed. However, hydrogen gas is colorless, odorless, highly volatile, and flammable. Explosion is very easy to occur when hydrogen gas concentration exceeds 4% in dry air; therefore, safety has always been a big issue in hydrogen storage and use [5, 6]. Developing a sensor for hydrogen gas is essential to monitor its amount for their applications in energy and environmental fields.

Metal oxide semiconductors in nanostructure have been widely used as the active materials for gas sensing because of their high catalytic activities and improved selectivity from the distinctive structure [7–10]. Cobalt oxide (Co_3O_4) is a *p*-type semiconductor and could be potentially employed for supercapacitors, electrochemical devices, and gas sensors due to its excellent electrocatalytic properties, high biocompatibility, and low cost [11–16]. A variety of harmful and toxic gases were detected using Co_3O_4 nanoparticles, such as volatile organic compounds (VOCs), H_2S, and NH_3 [17–20]. To improve the catalytic effectiveness and stability of Co_3O_4 nanoparticles, the design of novel nanostructures and hybrid nanomaterials based on Co_3O_4 nanoparticles is highly in demand.

Carbon nanotubes (CNTs) have shown the effects on the enhancement in catalytic activity for metal oxide gas sensing owing to the distinguished physical and chemical properties, such as excellent mechanical strength, thermal stability, hydrophilicity and stability, and electrical conductivity [21–24], because of their unique surface structures. There are many oxygen-containing groups (–COOH), graphite, and defects on the surface structures of CNTs from acidized treatment [25–27]. Zhang and coworkers showed that the CNTs could reduce the reaction temperature and enhance the gas sensitivity to CO gas for a metal oxide gas sensing system [28, 29]. Nguyen synthesized CNT films via CVD

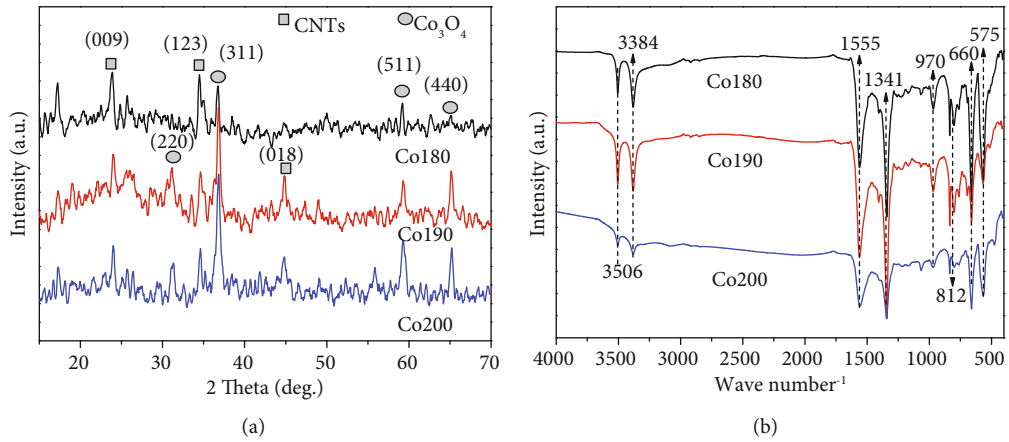

(a) (b)

Figure 1: (a) XRD patterns of CNT-Co_3O_4 composites. (b) FT-IR spectra of CNT-Co_3O_4 composites synthesized by a hydrothermal method at different temperatures.

and displayed fast response and high sensitivity for NH_3 sensing [30, 31]. CNTs also have been applied in the NO_2 gas sensor, and the NO_2 surface reaction can be explained by NO and NO_3 which are produced on the surface [32–34].

In this work, Co_3O_4 nanoparticles were successfully loaded onto the polyethylenimine (PEI) modifed CNTs via a hydrothermal method [28, 35]. The functional groups on the sidewalls of CNTs benefited from the binding of Co^{2+} ions or Co_3O_4 nanoparticles onto the CNTs. The Co_3O_4 nanoparticles were highly dispersed with the PEI-CNTs displaying high conductivity and uniform contact with hydrogen. The prepared hybrid material was integrated on the surface of a planar interdigitated gold electrode for hydrogen detection, and the results showed that PEI-CNTs did improve the gas sensing performance. The composite gas sensor exhibits perfect sensitivity, selectively, and response speed upon exposure to H_2 at room temperature.

2. Experiment

2.1. Syntheses of CNT-Co_3O_4 Nanomaterials. The CNT-Co_3O_4 composite materials were synthesized via a hydrothermal method. CNTs (Shenzhen Nanotech Port Co. Ltd., diameter: 30–80 nm, length: 5–30 μm) were functionalized firstly by acid treatment in the solution ($HNO_3 : H_2SO_4$ in a 1 : 3 (v/v) ratio). 80 mL of 0.03 mg/mL CNTs was added in 20 mL of 2 mg/mL PEI (branched PEI, Mw = 600, Cheng Du Micxy Chemical Co., Ltd.) under magnetic stirring, and the pH value of the solution was kept at 9.0. Subsequently, 20 mL of 2 mg/mL $Co(NO_3)_2{\cdot}6H_2O$ (Tianjin Regent Chemical, Tianjin, China) was added to the above mixed solution during stirring. After that, saturated sodium hydroxide solution was slowly added into the mixed solution to adjust the pH to 13. The air flow was set to the solution with 50 mL/min for 24 h. Then, the mixed solution was exfoliated by ultrasonication at a power of 100 W for 1 h, and then, the mixed solution was placed still for 24 h at room temperature. A black precipitate was filtered and washed with distilled water to neutral. Lastly, the precipitate was dispersed in distilled water and poured into the Teflon-lined stainless steel autoclave. Hydrothermal synthesis was conducted at 180, 190, and 200°C for 3 h, respectively. The obtained CNT-Co_3O_4 composites were named as Co180, Co190, and Co200, respectively.

2.2. Characterization. The crystalline structures of the products was characterized by X-ray powder diffraction (XRD, D/max-III B-40 kV, Japan, Cu-Kα radiation, $\lambda = 1.5406$ Å). The Fourier transform infrared (FT-IR) spectra were acquired with the FT-IR spectrometer (PerkinElmer Spectrometer, KBr pellet technique). The morphology of the synthesized samples were investigated using TEM (JEOL-JEM-2100, 200 kV).

2.3. Sensor Fabrication and Electrochemical Performance Measurements. The CNT-Co_3O_4 materials were dispersed in ethanol to form a suspension. The suspension was drop-casted to cover the surface of a planar interdigitated gold electrode on a ceramic substrate. Then, the electrode was dried in a vacuum oven at 80°C for 3 h. The electrochemical performances of the sensor were measured in a chamber with a gas flow apparatus. The electrical resistance of the sensor was measured using a computer-controlled multimeter for filtering signals (50 Hz ± 5%, Shanghai, China). During the gas sensing test, a certain volume of H_2 (99.9%, Dalian Great Special Gas Co., Ltd.) was injected with air at room temperature (25°C) in a relative humidity (RH) of around 45%. The response of the sensor was defined as the change of resistance in the two different gas circumstances:

$$S = \frac{R_g}{R_a}, \tag{1}$$

where R_g is the resistance in the tested gas and R_a is the resistance in air.

3. Results and Discussion

3.1. Structure Characterizations. The XRD diffraction and the FT-IR spectra of CNT-Co_3O_4 composites are shown in Figures 1(a) and 1(b), respectively. In the XRD patterns shown in Figure 1(a), two types of peaks can be indexed.

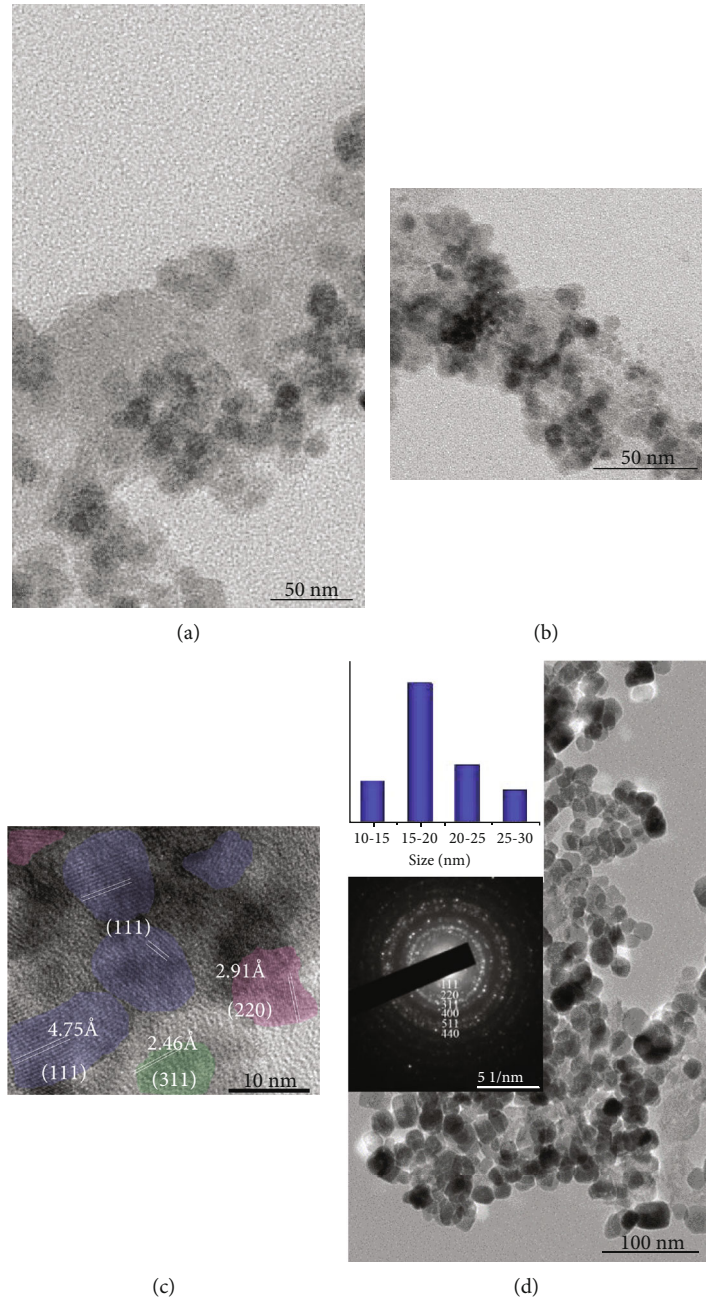

Figure 2: TEM characterization of CNT-sCo_3O_4 composite materials fabricated via the hydrothermal method at 180, 190, and 200°C: low-magnification and high-resolution TEM images of Co180 (a) and Co190 (b, c) and low-magnification TEM image and SAED of Co200 (d).

Diffraction peaks at 23.9°, 34.3°, and 44.7° can be indexed as the (009), (123), and (018) planes of the functional CNTs (JCPDS no. 74–2328, JCPDS no. 50–1086), and the d-spacings were calculated as 3.72, 2.61, and 2.03 Å, respectively. The XRD spectra showed a face-centered cubic Co_3O_4 phase with the corresponding peaks at 31.2°, 36.8°, 59.3°, and 65.2° (JCPDS no. 42–1467) to the planes of (220), (311), (511), and (440). Furthermore, there are no obvious (220) and (440) peaks existing in the Co180. From the XRD of CNT-Co_3O_4, we can find that the width at the half peak height of the same crystal plane is also different, indicating that the crystallinity and grain size of Co_3O_4 were influenced by the hydrothermal temperature. In addition, the high purity of the CNT-Co_3O_4 composites can be proven because of the two types of peaks.

The FT-IR spectra of CNT-Co_3O_4 composite materials are shown in Figure 1(b). The broad peak around 3506 and 3384 cm^{-1} would be attributed to the N–H stretch of secondary and primary amines of PEI in samples [36]. The peak at 1557 cm^{-1} is attributed to the C–C stretching vibration in CNTs [37], suggesting the CNTs presenting in the nanocomposites. CH_2 wagging from 1100 to 1500 cm^{-1} is a typical mode of PEI [28]. The peak stretching from 990 to 910 cm^{-1} and wagging from 840 to 800 cm^{-1} can be attributed to the unsaturated hydrocarbon (=C–H) of CNTs. The sharp peaks at 575 and 660 cm^{-1} are attributed to the

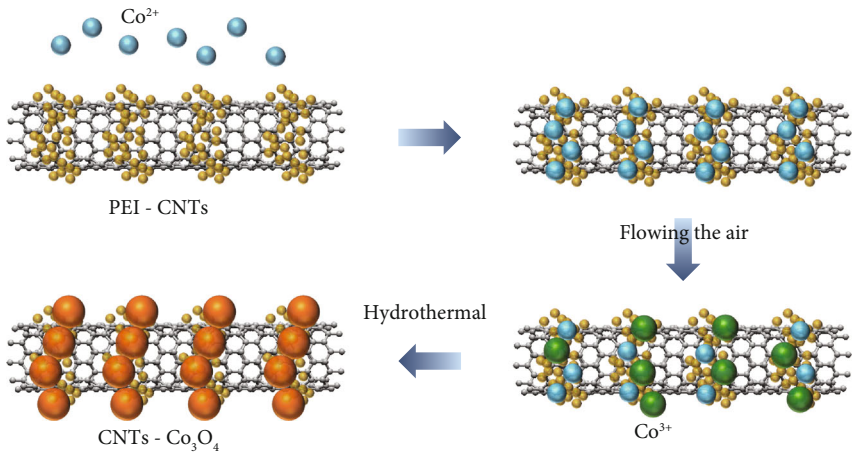

Figure 3: Scheme of the growth mechanism of the CNT-Co_3O_4 composite.

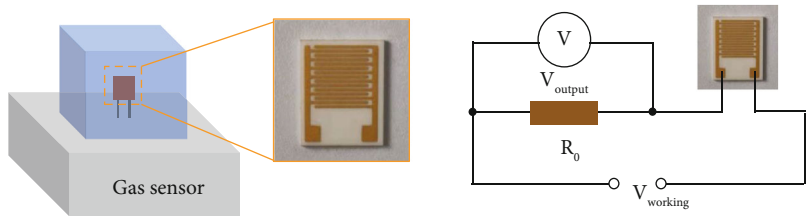

Figure 4: Sketches of the hydrogen sensor and the experimental circuit.

Co(III)–O and Co(II)–O stretching vibrations of Co_3O_4 [38]. Hence, through the FT-IR characterization, it presents that PEI-CNTs and Co_3O_4 nanoparticles have been successfully combined.

Figure 2 shows the TEM and HRTEM images of CNT-Co_3O_4 composite materials fabricated via the hydrothermal method at 180°C, 190°C, and 200°C. Figures 2(a)–2(d) show that Co_3O_4 nanoparticles were integrated onto the surface of CNTs, forming the CNT-Co_3O_4 composite materials with different densities of Co_3O_4 nanoparticles on CNTs. Figure 2(a) displays relative loose distribution of the aggregated Co_3O_4 nanoparticles on CNTs of the Co180 nanocomposite. Figure 2(b) shows that the aggregated Co_3O_4 nanoparticles were densely distributed on the CNTs. The HRTEM image in Figure 2(c) further shows the dense Co_3O_4 nanoparticles in different predominated crystal facets of (111), (220), and (311) with corresponding lattice d-spacing distance of 4.75, 2.91, and 2.46, respectively. The Co_3O_4 nanoparticles obtained at 190°C presented relatively large size (10–12 nm), while at the hydrothermal temperature of 200°C, it can be found from Figure 2(d) that Co_3O_4 nanoparticles almost fully covered the surface of CNTs. The SAED pattern of the Co200 nanocomposite displays the polycrystalline of Co_3O_4 with crystal planes of (111), (220), (311), (400), (511), and (440). The size distribution of Co_3O_4 nanoparticles in the Co200 nanocomposite was calculated, as shown in the inset of Figure 2(c). Relative large size distribution was found, and most of the Co_3O_4 nanoparticles were within the range of 15–20 nm. We found that the hydrothermal synthesis temperature would be able to control the size of Co_3O_4 nanoparticles and the coverage density of Co_3O_4 nanoparticles on CNT surfaces. Of the three synthetic temperatures, it shows the uniform size and morphology for the Co_3O_4 nanoparticles formed at 190°C.

The hypothesis of the formation mechanism for the nanocomposites is proposed in Figure 3. The CNTs after acid treatment can be endowed a large amount of moieties of –COOH and –OH, which improves the dispersion of CNTs and enables the modification with PEI. In our work, the PEI would bond to the $–COO^-$ groups of CNTs after both are mixed in the aqueous solution under pH 9; thus, PEI would be uniformly modified on the surface of the CNTs (step 1). The Co^{2+} from the precursor is easily dissociated and positively charged in aqueous solution. Then, we monitor the pH of the solution to 13 to unprotonate the PEI, so the Co^{2+} would be bonded to unprotonated PEI on the surface of CNTs and the Co^{2+} is functionalized onto CNT surfaces uniformly via PEI-CNTs (step 2). When air is introduced into the solution, Co^{2+} is oxidized to Co^{3+} gradually (step 3). The subsequent hydrothermal treatment at high temperature allows the in situ formation of Co_3O_4 nanoparticles on the surface of CNTs (step 4).

3.2. Gas Sensing Testing. The response of CNT-Co_3O_4 materials to H_2 gas was investigated through measuring the resistance versus time over two multifinger electrodes (size: 10 × 8 × 0.15 mm) at room temperature, as shown in Figure 4.

Figure 5 presents the H_2 gas sensing performance of CNT-Co_3O_4 nanocomposite materials, Co180, Co190, and Co200, respectively. The concentration range of H_2gas was adjusted from 1000 ppm to 30 ppm. The nanocomposite of CNTs-Co_3O_4 can play a role as the *p*-type semiconductor with the hole as the carrier. When a *p*-type semiconductor contacts

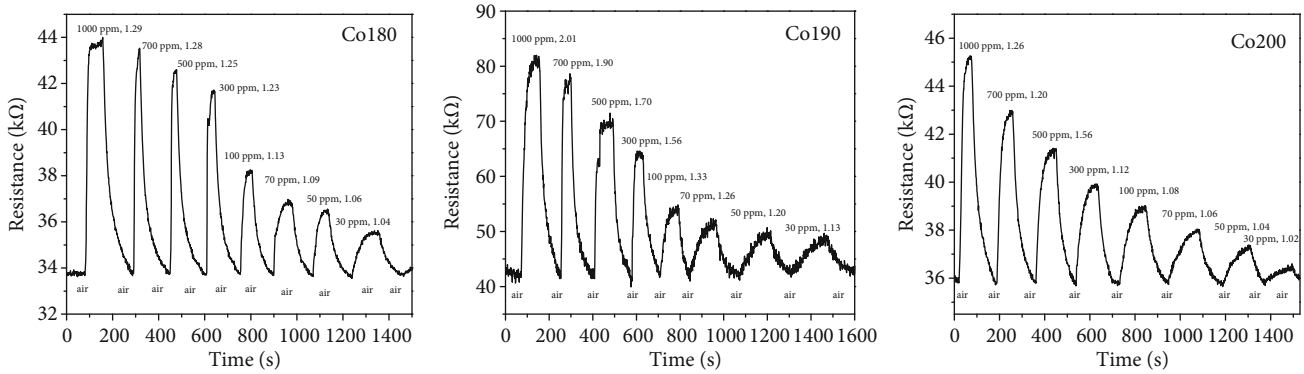

Figure 5: Dynamic response-recovery curves of the Co180, Co190, and Co200 thin film sensors to H_2 at room temperature, respectively.

with the reducing gas, the reduction interaction between them would produce electrons and the *p*-type semiconductor would accept the electron; thus, the resistance of the semiconductor would be increased. In Figure 5, we can see that the resistance of the CNT-Co_3O_4 nanocomposite increased when the air with H_2 passed through while its resistance dropped to the original value when air was introduced without H_2. The sensitivity decreases with the decrease in the concentration of the target gas, respectively, at room temperature. It is shown that the sensing response varies with the change in the concentration of the analyte gas.

By comparing the results shown in Figure 5, it can be seen that the response to H_2 is significantly higher for Co190 than the response to H_2 for Co180 and Co200 at room temperature. The response to the 1000 ppm H_2 for the nanocomposite Co190 presents the highest resistance, 81.9 kΩ, which is 2.01 times higher than the original resistance value. The response of the Co190 to the H_2 concentration of 30 ppm decreased, and the increased resistance is 1.13 times higher than the original value at room temperature. For the nanocomposite of Co200, the factor of the increased resistance decreased to 1.26 with 1000 ppm H_2. Hence, the nanocomposite of Co190 exhibited the highest sensing sensitivity among all three nanocomposite materials.

Furthermore, the CNT-Co_3O_4 nanocomposites fabricated at different hydrothermal temperatures displayed remarkably different effects on the recovery process of gas sensors. The possible reasons can be ascribed to the following aspects: (i) the Co_3O_4 nanoparticles were better dispersed on the surface of CNTs at low temperature and the Co_3O_4 nanoparticles were in relatively uniform size (shown in Figures 2(a) and 2(b)) and (ii) higher synthesis temperature caused large size of the Co_3O_4 nanoparticles and wide size distribution. Moreover, higher hydrothermal temperature induced severe nanoparticles' aggregation and complete coverage on the surface of CNTs (shown in Figure 2(c)). This resulted in a low surface-area-to-volume ratio, which decreased the surface area of exposure to target gas for response.

The roles of the CNTs and PEI for the sensing performance of the nanocomposite materials were investigated as well. The sensing response to H_2 of the pure Co_3O_4 nanoparticles, nanocomposite of Co_3O_4-PEI without CNTs, and nanocomposite of Co_3O_4-CNTs without PEI is shown in Figure 6. It has been found that without CNTs or PEI in the nanomaterial, the sensor exhibited significantly lower response than that of the nanocomposite of Co_3O_4-CNTs with PEI. It could be related to the coupling effect between the Co and CNTs, which had been proposed to contribute to the enhanced oxygen reduction ability [28]. In the Co_3O_4/PEI-CNT composite, when the CNT architecture was employed as conducting scaffolds in a Co_3O_4 semiconductor-based sensor, it not only prevents Co_3O_4 nanoparticles from aggregation but can also boost the electron transfer efficiency. PEI provided high-density homogeneous functional groups on the CNTs' sidewalls for binding Co_3O_4 nanoparticles. Meanwhile, PEI is helpful for high-density dispersion of Co_3O_4 grains and enhances the interaction between Co_3O_4 grains and CNTs and improves the transport of the carriers to the surface [39, 40]. Therefore, it could be concluded that the PEI played an important role in the sensing performance of the nanocomposites.

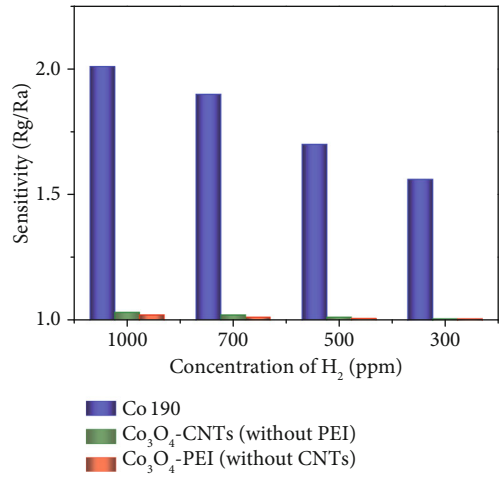

Figure 6: Comparison of sensitivities of the sensors using Co190, Co_3O_4-PEI (without CNTs), and Co_3O_4-CNTs (without PEI) to 300–1000 ppm H_2 at room temperature.

We also evaluated the sensing selectivity of the nanocomposites of CNT-Co_3O_4 to H_2 with the interferences such as ethanol, methanol, hydrogen, benzene, and acetone, as shown in Figure 7(a). The response of the sensor to 1000 ppm H_2 was

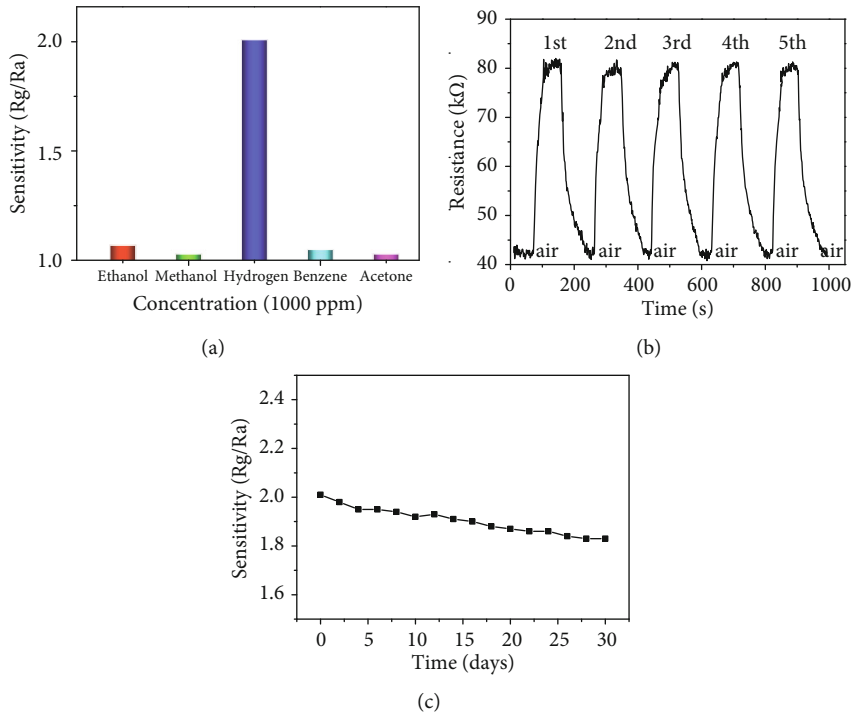

Figure 7: (a) Selectivity of the response of the CNT-Co_3O_4 sensor to 1000 ppm of ethanol, methanol, hydrogen, benzene, and acetone at room temperature. (b) Cycling stability curves of dynamic response-recovery and (c) long-term stability response of the CNT-Co_3O_4 sensor to 1000 ppm H_2 at room temperature.

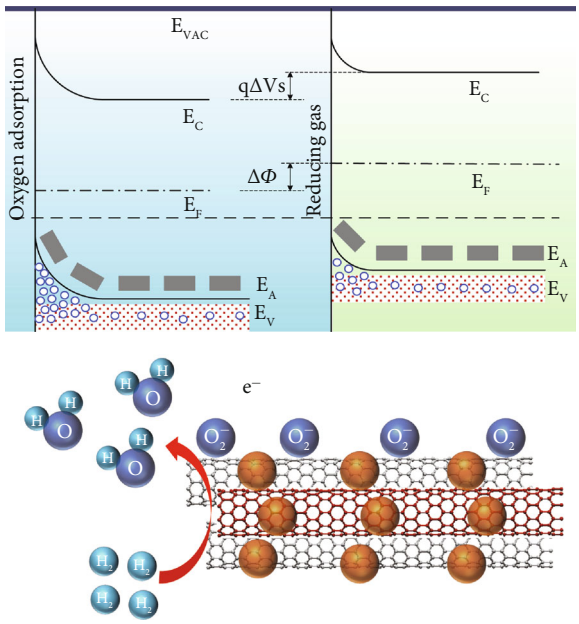

Figure 8: The structure and energy band model of the conductive mechanism in the air and reducing gas.

highest and 3–4 times higher than the responses to the other gases at the same concentration, suggesting an excellent selectivity to H_2 at room temperature.

To validate the sensing reliability and long-term stability of the CNT-Co_3O_4 composite sensor, we repeated the measurement of the dynamic response-recovery five times and tested the sensibility for 30 days. The repeatability of response and recovery curves shows the excellent repeatability in five consecutive experiments, as shown in Figure 7(b). After 30 days of long-term stability testing, the sensitivity of the sensor dropped from an initial 2.01 to 1.83; it retained 91.04% of its initial response, as shown in Figure 7(c). Therefore, CNTs-Co_3O_4 displays potentials in a sensor and wide range of application prospects for an H_2 sensor.

3.3. Gas Sensing Mechanism. The gas sensing mechanism of the metal oxide nanoparticles is strongly related to surface reactions [41], and chemisorbed oxygen also makes important contribution to the sensing mechanism. In general, the chemisorbed oxygen species of O_2^-, O^-, and O^{2-} can be formed at <150°C, 150~400°C, and >400°C, respectively. Because of the electrostatic interaction between the oppositely charged species, the adsorption of oxygen anions onto *p*-type oxide semiconductors induces the formation of hole accumulation layers. An energy band conduction model was used for the *p*-type oxide semiconductor as the gas sensors [7]. Figure 8 shows the structure and energy band model of the conductive mechanism in the air and reducing gas. When the *p*-type oxide semiconductor was exposed to the air, ambient oxygen can extract electrons from the valence band and form oxygen ions. It can increase the concentration of the holes, forming the hole accumulation layers. It can be depicted that the energy bands exhibited an upward band bending, of which length is the thickness of the hole accumulation layers. When the *p*-type oxide semiconductor is exposed to the reducing gas, the oxygen ions on the surface would be reacted. The decrease in the concentration of the holes, described in the energy band

representation as a downward band bending ($q\Delta Vs = \Delta\Phi$ in Figure 8), results in the increase in the resistance of the gas sensor. Hence, in our study, the ambient oxygen is absorbed on the surface of the CNTs-Co_3O_4 and traps the electrons at the surface as the oxygen ions (O_2^-) in the room temperature (2). When the CNT-Co_3O_4 was exposed under the ambient H_2, the reaction between reducing gas and oxygen ions (O_2^-) can result in the increase in the resistance of the CNT-Co_3O_4 gas sensor (3).

$$O_2 + e^- \leftrightarrow O_2^- \quad (2)$$

$$H_2 + O_2^- \leftrightarrow H_2O + e^- \quad (3)$$

4. Conclusion

In summary, the CNT-Co_3O_4 nanocomposites with highly dispersed Co_3O_4 were fabricated via the hydrothermal method. The CNT-Co_3O_4 nanocomposites display excellent sensing sensitivity, selectivity, and stability at room temperature to H_2 gas. CNTs play multiple roles in the sensing performance, not only offering the Co_3O_4 substrates to avoid its aggregation but also providing perfect migration of the electron pathway via the synergetic chemical coupling effect between Co_3O_4 and CNTs. PEI also contributes to improving the performance of H_2 sensors. Hence, the CNT-Co_3O_4 composites represent a potential application prospect in H_2 detection.

Data Availability

The experimental data used to support the findings of this study are included within the article.

Conflicts of Interest

The authors declare that they have no conflicts of interest.

Acknowledgments

This research was funded by the National Natural Science Foundation of China grant (No. 61905105), Guangdong Universities (advanced PVD coating and metal surface modification technology innovation team), Special Fund for Science and Technology Innovation Strategy of Guangdong Province (2020A0505100059), Natural Science Foundation of Guangdong Province (2021A1515011928), Guangdong Universities Innovation Project (No. 2020KTSCX073), and Zhanjiang Science and Technology Project (No. 2019A01044).

References

[1] V. T. Da Silva, T. S. Mozer, D. da Costa Rubim Messeder dos Santos, and A. da Silva César, "Hydrogen: trends, production and characterization of the main process worldwide," *International Journal of Hydrogen Energy*, vol. 42, no. 4, pp. 2018–2033, 2017.

[2] I. Staffell, D. Scamman, A. Velazquez Abad et al., "The role of hydrogen and fuel cells in the global energy system," *Energy & Environmental Science*, vol. 12, no. 2, pp. 463–491, 2019.

[3] F. Dawood, M. Anda, and G. M. Shafiullah, "Hydrogen production for energy: an overview," *International Journal of Hydrogen Energy*, vol. 45, no. 7, pp. 3847–3869, 2020.

[4] J. O. Abe, A. P. I. Popoola, E. Ajenifuja, and O. M. Popoola, "Hydrogen energy, economy and storage: review and recommendation," *International Journal of Hydrogen Energy*, vol. 44, no. 29, pp. 15072–15086, 2019.

[5] B. Sharma, A. Sharma, and J. S. Kim, "Recent advances on H_2 sensor technologies based on MOX and FET devices: a review," *Sensors and Actuators B: Chemical*, vol. 262, pp. 758–770, 2018.

[6] E. Herkert, F. Sterl, N. Strohfeldt, R. Walter, and H. Giessen, "Low-cost hydrogen sensor in the ppm range with purely optical readout," *ACS Sensors.*, vol. 5, no. 4, pp. 978–983, 2020.

[7] N. Barsan and U. Weimar, "Conduction model of metal oxide gas sensors," *Journal of Electroceramics*, vol. 7, no. 3, pp. 143–167, 2001.

[8] A. Dey, "Semiconductor metal oxide gas sensors: a review," *Materials Science and Engineering: B*, vol. 229, pp. 206–217, 2018.

[9] P. T. Moseley, "Progress in the development of semiconducting metal oxide gas sensors: a review," *Measurement Science and Technology*, vol. 28, no. 8, article 082001, 2017.

[10] N. Joshi, T. Hayasaka, Y. Liu, H. Liu, O. N. Oliveira, and L. Lin, "A review on chemiresistive room temperature gas sensors based on metal oxide nanostructures, graphene and 2D transition metal dichalcogenides," *Microchimica Acta*, vol. 185, no. 4, p. 213, 2018.

[11] N. Ortiz Peña, D. Ihiawakrim, M. Han et al., "Morphological and structural evolution of Co_3O_4 nanoparticles revealed by in situ electrochemical transmission electron microscopy during electrocatalytic water oxidation," *ACS Nano*, vol. 13, no. 10, pp. 11372–11381, 2019.

[12] X. Ren, H. Fan, J. Ma, C. Wang, M. Zhang, and N. Zhao, "Hierarchical Co_3O_4/PANI hollow nanocages: synthesis and application for electrode materials of supercapacitors," *Applied Surface Science*, vol. 441, pp. 194–203, 2018.

[13] P. Jiang, H. Zhang, C. Chen et al., "Co_3O_4–SnO_2 nanobox sensor with a PN junction and semiconductor-conductor transformation for high selectivity and sensitivity detection of H_2S," *CrystEngComm*, vol. 19, no. 38, pp. 5742–5748, 2017.

[14] T. H. Kim, J. W. Yoon, and J. H. Lee, "A volatile organic compound sensor using porous Co_3O_4 spheres," *Journal of the Korean Ceramic Society*, vol. 53, no. 2, pp. 134–138, 2016.

[15] P. G. Choi, T. Fuchigami, K. I. Kakimoto, and Y. Masuda, "Effect of crystal defect on gas sensing properties of Co_3O_4 nanoparticles," *ACS Sensors*, vol. 5, no. 6, pp. 1665–1673, 2020.

[16] K. A. Dehno, "Synthesis, characterization and optical properties of Co_3O_4 nanoparticles," *Asian Journal of Nanosciences and Materials*, vol. 2, no. 2, pp. 186–190, 2019.

[17] S. Todorova, J. L. Blin, A. Naydenov et al., "Co_3O_4-MnO_x oxides supported on SBA-15 for CO and VOCs oxidation," *Catalysis Today*, vol. 357, pp. 602–612, 2020.

[18] Y. Sun, Z. Wang, W. Wang et al., "Electrospinning preparation of Pd@Co_3O_4-ZnO composite nanofibers and their highly enhanced VOC sensing properties," *Materials Research Bulletin*, vol. 109, pp. 255–264, 2019.

[19] P. L. Quang, N. D. Cuong, T. T. Hoa et al., "Simple post-synthesis of mesoporous p-type Co_3O_4 nanochains for enhanced H_2S gas sensing performance," *Sensors and Actuators B: Chemical*, vol. 270, pp. 158–166, 2018.

[20] X. Xie, Y. Li, Z. Q. Liu, M. Haruta, and W. Shen, "Low-temperature oxidation of CO catalysed by Co_3O_4 nanorods," *Nature*, vol. 458, no. 7239, pp. 746–749, 2009.

[21] J. G. Thangamani, K. Deshmukh, K. Kumar Sadasivuni et al., "Recent advances in electrochemical biosensor and gas sensors based on graphene and carbon nanotubes (CNT) - a review," *Advanced Materials Letters*, vol. 8, no. 3, pp. 196–205, 2017.

[22] R. H. Baughman, A. A. Zakhidov, and W. A. De Heer, "Carbon nanotubes - the route toward applications," *Science*, vol. 297, no. 5582, pp. 787–792, 2002.

[23] M. M. Rana, D. S. Ibrahim, M. R. Mohd Asyraf, S. Jarin, and A. Tomal, "A review on recent advances of CNTs as gas sensors," *Sensor Review*, vol. 37, no. 2, pp. 127–136, 2017.

[24] Y. M. Wong, W. P. Kang, J. L. Davidson, A. Wisitsora-At, and K. L. Soh, "A novel microelectronic gas sensor utilizing carbon nanotubes for hydrogen gas detection," *Sensors and Actuators B: Chemical*, vol. 93, no. 1-3, pp. 327–332, 2003.

[25] P. Qi, C. Zhao, R. Wang, T. Fei, and T. Zhang, "High-performance QCM humidity sensors using acidized-multiwalled carbon nanotubes as sensing film," *IEEE Sensors Journal*, vol. 18, no. 13, pp. 5278–5283, 2018.

[26] S. Mallakpour and E. Khadem, "Carbon nanotube-metal oxide nanocomposites: Fabrication, properties and applications," vol. 302, no. 1, pp. 344–367, 2016.

[27] S. Liu, Z. Wang, Y. Zhang, C. Zhang, and T. Zhang, "High performance room temperature NO_2 sensors based on reduced graphene oxide-multiwalled carbon nanotubes-tin oxide nanoparticles hybrids," *Sensors and Actuators B: Chemical*, vol. 211, no. 2, pp. 318–324, 2015.

[28] G. Zhang, L. Dang, L. Li, R. Wang, H. Fu, and K. Shi, "Design and construction of Co_3O_4/PEI-CNTs composite exhibiting fast responding CO sensor at room temperature," *CrystEngComm*, vol. 15, no. 23, pp. 4730–4738, 2013.

[29] Y. Lin, K. Kan, W. Song et al., "Controllable synthesis of Co_3O_4/polyethyleneimine-carbon nanotubes nanocomposites for CO and NH_3 gas sensing at room temperature," *Journal of Alloys and Compounds*, vol. 639, pp. 187–196, 2015.

[30] L. Q. Nguyen, P. Q. Phan, H. N. Duong, C. D. Nguyen, and L. H. Nguyen, "Enhancement of NH3 gas sensitivity at room temperature by carbon nanotube-based sensor coated with Co nanoparticles," *Sensors*, vol. 13, no. 2, pp. 1754–1762, 2013.

[31] L. H. Nguyen, T. V. Phi, P. Q. Phan, H. N. Vu, C. Nguyen-Duc, and F. Fossard, "Synthesis of multi-walled carbon nanotubes for NH_3 gas detection," *Physica E: Low-dimensional Systems and Nanostructures*, vol. 37, no. 1-2, pp. 54–57, 2007.

[32] S. W. Lee, W. Lee, Y. Hong, G. Lee, and D. S. Yoon, "Recent advances in carbon material-based NO_2 gas sensors," *Sensors and Actuators B: Chemical*, vol. 255, no. 2, pp. 1788–1804, 2018.

[33] D. Ma, Y. Su, T. Tian et al., "Highly sensitive room-temperature NO_2 gas sensors based on three-dimensional multiwalled carbon nanotube networks on SiO_2 nanospheres," *ACS Sustainable Chemistry & Engineering*, vol. 8, no. 37, pp. 13915–13923, 2020.

[34] H. Song, K. Li, and C. Wang, "Selective detection of NO and NO_2 with CNTs-based ionization sensor array," *Micromachines*, vol. 9, no. 7, p. 354, 2018.

[35] O. Alev, A. Kılıç, Ç. Çakırlar, S. Büyükköse, and Z. Z. Öztürk, "Gas sensing properties of p-Co_3O_4/n-TiO_2 nanotube heterostructures," *Sensors*, vol. 18, no. 4, p. 956, 2018.

[36] E. Yoo, L. Gao, T. Komatsu et al., "Atomic hydrogen storage in carbon nanotubes promoted by metal catalysts," *The Journal of Physical Chemistry. B*, vol. 108, no. 49, pp. 18903–18907, 2004.

[37] L. Cao, M. Lu, and H.-L. Li, "Preparation of mesoporous nanocrystalline Co_3O_4 and its applicability of porosity to the formation of electrochemical capacitance," *Journal of the Electrochemical Society*, vol. 152, no. 5, p. A871, 2005.

[38] C. Nethravathi, S. Sen, N. Ravishankar, M. Rajamathi, C. Pietzonka, and B. Harbrecht, "Ferrimagnetic nanogranular Co_3O_4 through solvothermal decomposition of colloidally dispersed monolayers of α-cobalt hydroxide," *The Journal of Physical Chemistry. B*, vol. 109, no. 23, pp. 11468–11472, 2005.

[39] C. H. Kuo, W. Li, W. Song et al., "Facile synthesis of Co_3O_4@CNT with high catalytic activity for CO oxidation under moisture-rich conditions," *ACS Applied Materials & Interfaces*, vol. 6, no. 14, pp. 11311–11317, 2014.

[40] X. Zhang, H. Zhong, L. Xu et al., "Fabrication of Co_3O_4/PEI-GO composites for gas-sensing applications at room temperature," *Materials Research Bulletin*, vol. 102, pp. 108–115, 2018.

[41] G. Korotcenkov, "The role of morphology and crystallographic structure of metal oxides in response of conductometric-type gas sensors," *Materials Science and Engineering: B*, vol. 61, no. 1-6, pp. 1–39, 2008.